Probing biomechanical properties with a centrifugal force quartz crystal microbalance Supplementary Information

Aaron Webster,[1] Frank Vollmer,[1] and Yuki Sato[2]

[1] *Max Planck Institute for the Science of Light, Erlangen D-91058, Germany*

[2] *The Rowland Institute at Harvard, Harvard University, Cambridge, Massachusetts 02142, USA*

(Dated: Friday 5th September, 2014)

CONTENTS

S1. INTRODUCTION

This document is supplementary information to *Probing biomechanical properties with a centrifugal force quartz crystal microbalance*. Herein we give details on numerical simulations and further derivations which are referenced in the main text. Unless specified otherwise, all section, figure, table, and equation references pertaining to the supplement are prefixed by an "S", while references to the corresponding manuscript are not prefixed.

S2. SIMULATION DETAILS

Finite element simulations were carried out using the software `COMSOL Multiphysics 4.3 (4.3.0.233)` [1]. Though this software's source code is not available for scrutinous review, our implementation is generic and may be carried out using other software (e.g. `OpenFOAM` [2], `SU2` [3]). Unless otherwise stated, implementation specific information is applicable to `COMSOL`.

The simulation is done by solving the steady state incompressible Navier Stokes equations, neglecting turbulence, using finite element analysis in two dimensions

$$\rho\left(\dot{\mathbf{u}}\cdot\nabla\right)\dot{\mathbf{u}} = \nabla\cdot\left(-\rho\mathbf{I}+\eta\left(\nabla\dot{\mathbf{u}}+\left(\nabla\dot{\mathbf{u}}\right)^{\mathrm{T}}\right)\right)+\mathbf{F} \tag{S1}$$

$$\rho\nabla\cdot\dot{\mathbf{u}} = 0 \tag{S2}$$

where $\dot{\mathbf{u}}$ is flow velocity field, ρ is fluid density, η is dynamic viscosity, and $\mathbf{F}$ is the body force per unit volume. The computational domain is set up as shown in FIG. S1.

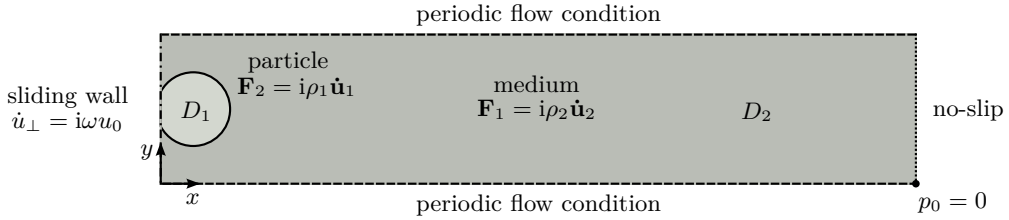

FIG. S1. Computational geometry for the simulation.

The left hand side (-·-·-) is a sliding wall and is given a tangential velocity of $\dot{u}_\perp = \mathrm{i}\omega u_0$, where $\omega = 2\pi f$ is the angular frequency of oscillation and $u_0 = 1 \times 10^{-2}\,\mathrm{nm}$ is its amplitude. The top and bottom (----) are given a periodic flow condition such that their pressure difference is zero. The right hand side (·····) has a zero-slip condition. The two materials 1, the particle, and 2, the medium in domains D_1 and D_2 are assigned a volume force $\mathbf{F} = \mathrm{i}\omega\rho\dot{\mathbf{u}}$, where ρ is the density of the material, (e.g. $\rho_1 = 1.06\,\mathrm{g\,cm^{-3}}$ for polystyrene and $\rho_2 = 1\,\mathrm{g\,cm^{-3}}$ for water). Finally. an initial pressure point constraint of $p_0 = 0$ is assigned to the point in the bottom right of the domain.

The sphere (or, more appropriately, cylinder in 2D) comprising D_1 with diameter d and radius r is located a distance $s > -r$, measured from the bottom of the sphere, from the oscillating boundary. If $s > 0$, the sphere does not make contact with the boundary. If $s \leq 0$, the sphere is truncated at the boundary resulting in a finite contact radius r_c. It is useful to sample in either domain, so we either sweep r_c or s, converting between them with

$$r_\mathrm{c}(s) = \sqrt{2r - s}\sqrt{s} \tag{S3}$$

$$s(r_\mathrm{c}) = \left(r - \sqrt{r^2 - r_\mathrm{c}^2}\right)\mathrm{sgn}(r_\mathrm{c}) \tag{S4}$$

The number density N_L was controlled by increasing or decreasing the height of the domain proportional to the size of the sphere.

The materials in the simulation are assigned a complex dynamic viscosity $\eta = \eta' - \mathrm{i}\eta''$. This is related to the complex bulk modulus $G = G' + \mathrm{i}G''$ by

$$\eta = \frac{G}{\mathrm{i}\omega} \tag{S5}$$

and the loss tangent, the angle between the real and imaginary components is

$$\tan\delta = \frac{G''}{G'} \tag{S6}$$

Specific to the stationary solver in `COMSOL`, in the `Study`→`Stationary Solver`→`Advanced` window, "Allow complex-valued output from functions with real input" was checked. This, coupled with the complex valued input for the body forces, will produce shear waves in the simulation.

The mesh settings were calibrated in `COMSOL` for fluid dynamics with a maximum mesh size of $1 \times 10^{-9}\,\mathrm{m}$ along the oscillating boundary. All other meshes were generated automatically. As for the size of the computational domain, we find that a height (parallel to the oscillating boundary) of $h = 2d$ and width (perpendicular to the oscillating boundary) $w = 2d$, minimum of 500 nm, produces consistent results with a minimum of error and computational resources.

It is important to note that, because the simulation is two dimensional, what is actually simulated are infinite cylinders rather than spheres. For Sauerbrey type viscoelastic films, the influence of this is negligible. However, for asperity contacts such as spheres, we find that the results, however qualitatively correct, do not always result in exact numerical agreement with experiment [4]. An extended simulation in three dimensions at some point is warranted.

S2.1. Contact Surface Density

In the main manuscript we plot shifts in Δf and $\Delta\Gamma$ as a function of a parameter called *contact surface density*, A_c. This allows one to compare shifts between particles with different radii. To be clear, we define A_c as the ratio of the

area of the sphere in contact with the oscillating boundary (twice the contact radius in 2D) to the area (length in 2D) of the domain. This means, for example, that for a domain with $h = 2d$, the maximum contact area will be d and the maximum value of $A_c = 0.5$

S2.2. Extracting Shifts

Shifts in frequency, Δf, and bandwidth (half-width at half maximum), $\Delta\Gamma$, are computed by evaluating the stress-speed ratio of the oscillating boundary according to the relationship

$$\frac{\Delta f + \mathrm{i}\Delta\Gamma}{f_\mathrm{F}} = \frac{\mathrm{i}}{\pi Z_\mathrm{q}} Z_\mathrm{L} = \frac{\mathrm{i}}{\pi Z_\mathrm{q}} \left\langle \frac{\sigma}{\dot{u}} \right\rangle \tag{S7}$$

where σ is the (complex) stress, $\dot{u}$ is the (complex) velocity, Z_L is the load impedance, and $\langle\ \rangle$ denotes a line average along the boundary. In `COMSOL`, and in the coordinates of FIG. S1, σ is `Total stress, y component` (`v`) and $\dot{u}$ is `Velocity field, y component`, (`spf.T_stressy`). Note that the stress speed ratio $\langle\sigma/\dot{u}\rangle$ is dimensionally equivalent to specific acoustic impedance, also called "shock impedance", sound pressure over velocity. In other words, the stress-speed ratio is the impedance of the film.

S2.3. Verification Examples

Here we check the validity of the numerical simulation with examples for which the QCM's response is well known.

S2.3.1. Evanescent Shear Wave

Setting up the model as described produces a shear wave which closely matches theory, as shown in FIG. S2. An analytic expression of the evanescent shear wave in a liquid has been reported [5] to be

$$\frac{u(z)}{u_0} = \exp\left(-\sqrt{\frac{\mathrm{i}\rho\omega}{\eta}}\, z\right) \tag{S8}$$

where $\eta = \eta' - \mathrm{i}\eta''$ is the complex viscosity, ρ is the density of the liquid, ω is the angular frequency of the QCM oscillation, and z is the spatial extension. The 1/e penetration depth δ is

$$\delta = -\left(\Im\left(\sqrt{\frac{\rho\omega}{\mathrm{i}\eta}}\right)\right)^{-1} \tag{S9}$$

With $\rho = 1\,\mathrm{g\,cm^{-3}}$ and $|\eta|^2 = 1\,\mathrm{mPa\,s}$, EQN. S9 predicts $\delta \approx 252\,\mathrm{nm}$. This is in good agreement with the simulation data, shown in FIG. S2.

S2.3.2. Semi-Infinite Viscoelastic Medium

A semi-infinite medium will produce a complex response described by [6] [7]

$$\frac{\Delta f + \mathrm{i}\Delta\Gamma}{f_\mathrm{F}} = \frac{\mathrm{i}}{\pi Z_\mathrm{q}} \sqrt{\rho G} \tag{S10}$$

$$= \frac{1}{\pi Z_\mathrm{q}} \frac{(-1+\mathrm{i})}{\sqrt{2}} \sqrt{\omega\rho\eta} \tag{S11}$$

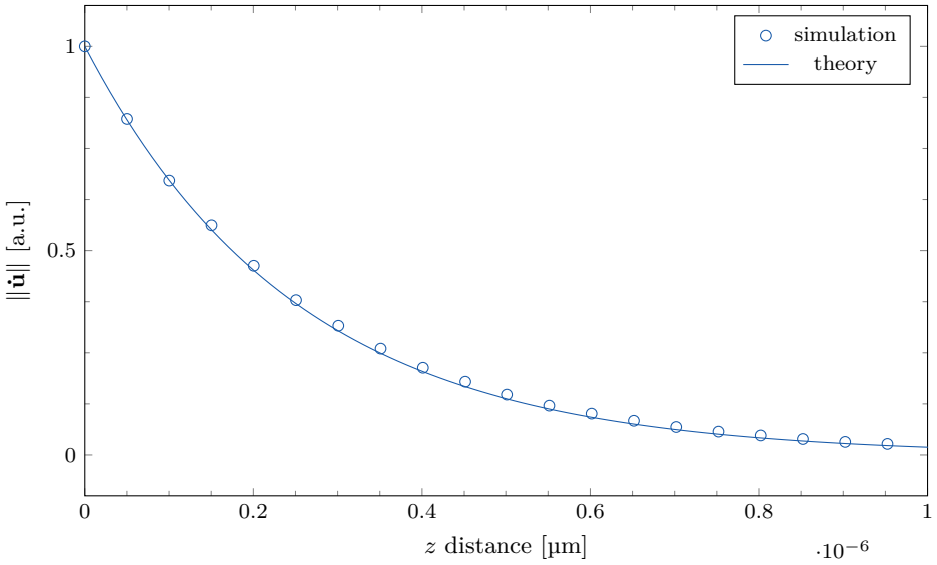

FIG. S2. QCM shear wave decay at 5 MHz, comparison between simulation and theory.

$f = \omega/(2\pi)$ is the frequency of the crystal, ρ and η are the density and viscosity of the medium in contact with the crystal, and ρ_q and μ_q are the density and shear modulus of quartz. This model applies for crystals with one side in contact with the viscoelastic material. This is related to the dynamic viscosity and shear modulus by

$$\frac{\Delta f + \mathrm{i}\Delta\Gamma}{f_\mathrm{F}} = \frac{\mathrm{i}}{\pi Z_\mathrm{q}} \frac{(-1+\mathrm{i})}{\sqrt{2}} \sqrt{\rho\omega\left(\eta' - \mathrm{i}\eta''\right)} \tag{S12}$$

$$= \frac{\mathrm{i}}{\pi Z_\mathrm{q}} \sqrt{\rho\left(G' + \mathrm{i}G''\right)} \tag{S13}$$

The simulation geometry was set as described in FIG. S1 but without D_1 (no sphere). Extracted values of Δf and $\Delta\Gamma$ are presented in FIG. S3 as a function of the viscosity η of medium 1. In FIG. S3(a) we sweep η' for a Newtonian fluid, $\eta'' = 0$. In FIG. S3(b) we model a non-Newtonian sample; $\eta' = 1\,\mathrm{mPa\,s}$ and η'' is swept. The excellent agreement with theory demonstrates that our simulation is applicable for a wide range of materials.

It is of note that our Navier-Stokes approach (which solves for $\dot{\mathbf{u}}$) does not converge in the limit of a perfectly elastic material, e.g. $G = G'$ or $\eta = \eta''$; these systems are typically solved for $\mathbf{u}$. It is perhaps possible to couple these two domains, but we have not attempted to do so.

S3. MECHANICAL MODEL

We have employed a mechanical model based on coupled oscillators shown in FIG. S4. Here the resonance of the QCM at $\omega_\mathrm{q}^2 = k_\mathrm{q}/m_\mathrm{q}$ is coupled to a mass m_L through a spring k_L and dashpot ξ_L. The spring and dashpot are not *actual* springs and dashpots, rather they are analogies for the coupling of two systems with different resonances in the small load approximation. The QCM itself has a small damping term, but it is small enough that we neglect it.

The derivation of this equation is described in detail in REF. [8]. Here we use the same equation but as a function of k_L, rather than that of the load resonance $\omega_\mathrm{L}^2 = k_\mathrm{L}/m_\mathrm{L}$; the former being more appropriate to our analysis. Using the small load approximation, the response of the system as a function of its coupling k_L is

$$\frac{\Delta f + \mathrm{i}\Delta\Gamma}{f_\mathrm{F}} = \frac{N_\mathrm{L}}{\pi \mathrm{Z}_\mathrm{q}} \frac{m_\mathrm{L}\omega_\mathrm{q}\left(k_\mathrm{L} + \mathrm{i}\omega_\mathrm{q}\xi_\mathrm{L}\right)}{m_\mathrm{L}\omega_\mathrm{q}^2 - \left(k_\mathrm{L} + \mathrm{i}\omega_\mathrm{q}\xi_\mathrm{L}\right)} \tag{S14}$$

where Z_q is the acoustic impedance of AT cut quartz, f_F is the fundamental frequency of the resonator, and N_L is a number surface density (number per unit area) for discrete loads.

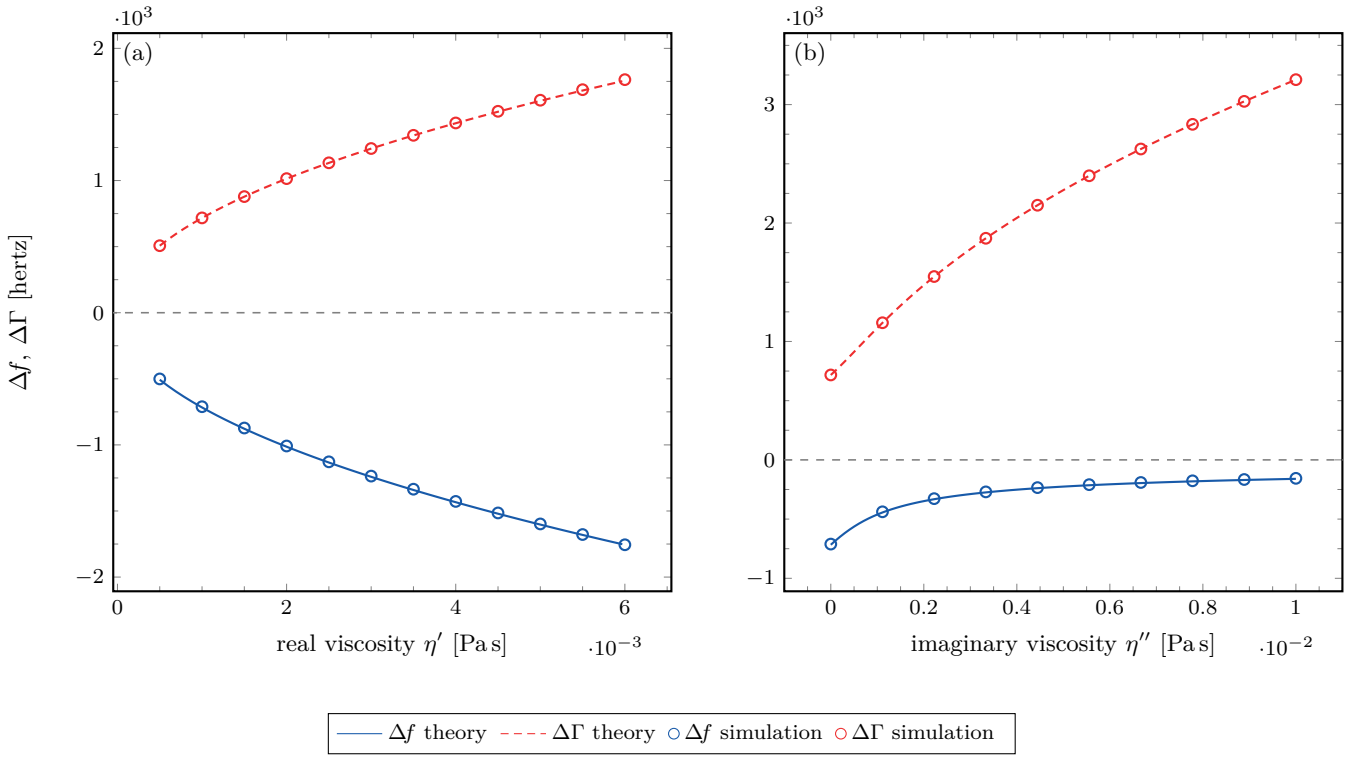

FIG. S3. Comparison of Δf and $\Delta\Gamma$ verses viscosity η for both the finite element simulation and EQN. S11. (a) $\eta'' = 0$ and η' is swept (a Newtonian liquid). (b) $\eta' = 1\,\mathrm{mPa\,s}$ and η'' is swept.

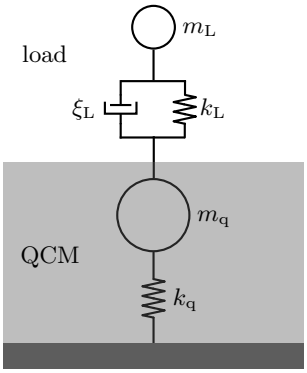

FIG. S4. Coupled oscillator mechanical model for QCM behavior.

FIG. S5 shows a comparison between the finite element simulation and a best fit of EQN. S14. Here the only free system parameter is ξ_L, which we find to be approximately $7.5 \times 10^{-7}\,\mathrm{N\,s\,m^{-1}}$. The domain of the fit is set by $A_\mathrm{c} = 0$ and the frequency zero crossing at $k_\mathrm{zc} = m_\mathrm{L}\omega_\mathrm{q}^2$.

Fitting is simplified with a parametric plot of $\Delta\Gamma$ verses Δf. For hard spheres this will form a circle with radius r_L,

$$\frac{r_\mathrm{L}}{f_\mathrm{F}} = \frac{N_\mathrm{L}}{\pi Z_\mathrm{q}} \frac{(m_\mathrm{L}\omega_\mathrm{q})^2}{2\xi_\mathrm{L}} \sqrt{1 + \left(\frac{\xi_\mathrm{L}}{m_\mathrm{L}\omega_\mathrm{q}}\right)^2} \tag{S15}$$

$$\approx \frac{N_\mathrm{L}}{\pi Z_\mathrm{q}} \frac{(m_\mathrm{L}\omega_\mathrm{q})^2}{2\xi_\mathrm{L}}, \quad \text{for } \xi_\mathrm{L} \ll 1 \tag{S16}$$

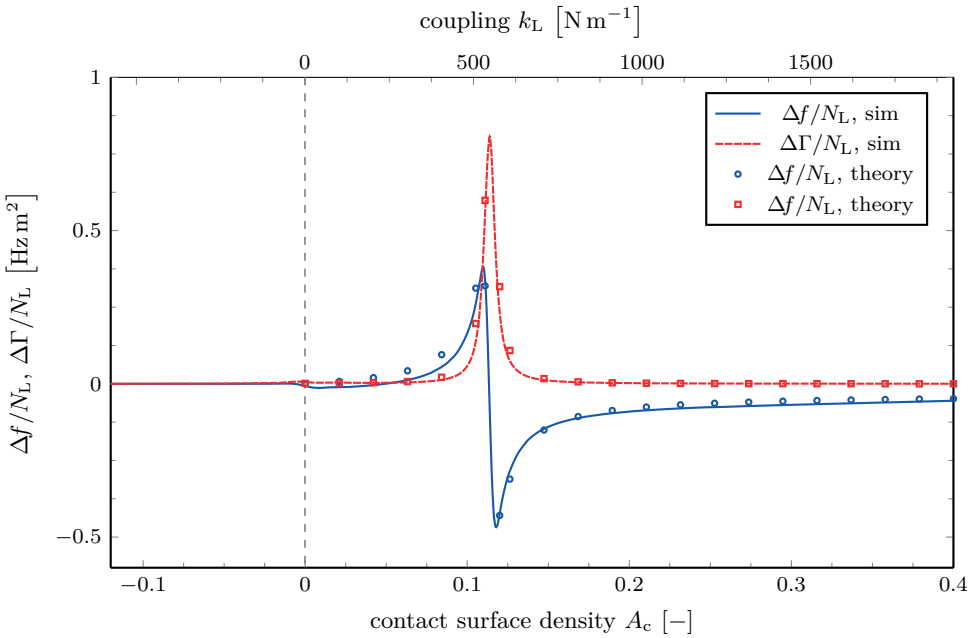

FIG. S5. Comparison between mechanical model and finite element simulation for a 10 µm polystyrene particle.

S4. NOISE AND COMPARISON TO QCM-D

Our experimental setup used a 25 mm diameter 5 MHz gold coated crystal in combination with an SRS QCM200 PLL based driver circuit and an external rubidium frequency standard. Typical of most QCM circuits, the QCM200 provides an output proportional to Δf, which we use directly in all discussions of Δf. However, unlike a QCM-D device which gives a "dissipation factor", D, defined in terms of the bandwidth $\Delta\Gamma$ as $D = 2\Delta\Gamma/f_F$, the QCM200 outputs the motional resistance R_m of the Butterworth van Dyke equivalent circuit. R_m is, related to the bandwidth Γ and the QCM-D dissipation D by

$$R_m = (4\pi L_m)\,\Gamma \tag{S17}$$
$$= (2\pi L_m f_F)\,D \tag{S18}$$

where L_m is the Butterworth van Dyke equivalent motional inductance. Because of the small load approximation, $\Delta f/f_F \ll 1$ and likewise $\Delta L/L_m \ll 1$, we can effectively treat L_m as a constant. [9] This value is typically in the range of 30 mH [10] [11] to 40 mH [12] [13] [14], with 40 mH being more common and the value we use in our analysis. At $L_m = 40$ mH, we find in water $R_m = 359\,\Omega$, which is within 1 % of the predicted value [6] of 357 Ω. In this sense, dissipation D and motional resistance R_m are independent but equivalent measures of the QCM bandwidth.

We have calculated the noise in Δf and R_m for the SRS QCM200 in our experiment and find it to be about 0.4 Hz (0.008 ppm) for Δf and 0.006 Ω (13 ppm) for R_m, corresponding to a signal to noise ratio of 110 dB. This is close to the manufacturer's specification [10] of 0.1 Hz for Δf and ±28 ppm for R_m. We have analyzed the noise separately for both the loading and unloading orientations of the crystal, as well as for different centrifuge spin speeds. We find no discernible difference in the noise between any of these cases. We did not at any point modify the centrifuge or bucket assembly in an attempt to try and reduce system noise.

In comparison, a typical QCM-D such as those sold by Q-Sense [15] will have noise of about 0.3 Hz in Δf and 0.2×10^{-6} in D at 5 MHz [16] [17]. Converting from R_m to D and vice-versa, we find the SRS QCM200 has an equivalent noise in D of 0.005×10^{-6} and the Q-Sense QCM-D an equivalent noise in motional resistance of 0.25 Ω. In terms of $\Delta\Gamma$, the Q-Sense QCM-D has a noise of 0.5 Hz and the SRS QCM200 0.01 Hz. Even though we stated that our chosen value for L_m gives R_m within 1 % of the predicted value for water, uncertainties in the value of L_m used for the R_m-$\Delta\Gamma$ conversion do not significantly affect this analysis for the range of L_m values quoted in the literature.

It is clear with this comparison that the SRS QCM200 PLL based driver and a QCM-D device are both measures of the same underlying physical phenomena taking place in a resonating quartz crystal. [9] Moreover, as exemplified by the discrete particle data in the main text, the QCM signal amplitudes increase further with the application of

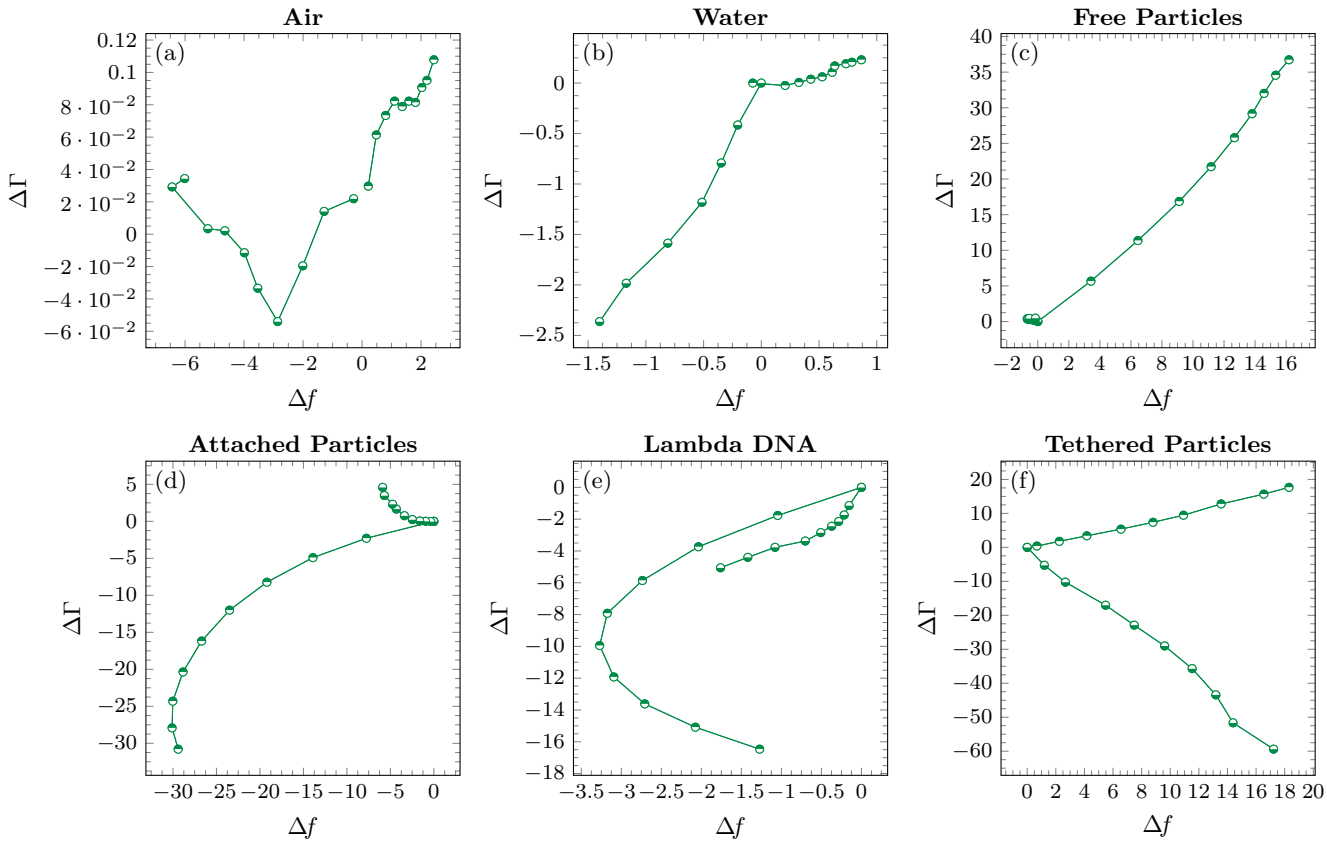

FIG. S6. Parametric representations of the load situations from the manuscript.

centrifugal force for the device reported here. It is important to note that the important aspect of the CF-QCM, the centrifugal force, is independent of the type of technique used to drive and monitor the quartz crystal. We therefore see no reason why our technique would not apply to all QCM based measurement techniques.

S5. PARAMETRIC REPRESENTATION

The different load situations depicted in the main manuscript are shown parametrically in FIG. S6.

[1] COMSOL Multiphysics. Comsol. Inc., Burlington, MA, http://www.comsol.com, 1994.

[2] Hrvoje Jasak, Aleksandar Jemcov, and Zeljko Tukovic. Openfoam: A c++ library for complex physics simulations. In International workshop on coupled methods in numerical dynamics, pages 1–20, 2007.

[3] Francisco Palacios, Michael R Colonno, Aniket C Aranake, Alejandro Campos, Sean R Copeland, Thomas D Economon, Amrita K Lonkar, Trent W Lukaczyk, Thomas WR Taylor, and Juan J Alonso. Stanford university unstructured (su2): An open-source integrated computational environment for multi-physics simulation and design. AIAA Paper, 287:2013, 2013.

[4] Ewa Vittorias, Michael Kappl, Hans-Jürgen Butt, and Diethelm Johannsmann. Studying mechanical microcontacts of fine particles with the quartz crystal microbalance. Powder Technology, 203(3):489–502, 2010.

[5] Claudia Steinem, Andreas Janshoff, and Matthew A Cooper. Piezoelectric sensors, volume 5. Springer, 2007.

[6] K. Keiji Kanazawa and Joseph G. Gordon. Frequency of a quartz microbalance in contact with liquid. Analytical Chemistry, 57(8):1770–1771, 1985.

[7] Stephen J Martin, Victoria Edwards Granstaff, and Gregory C Frye. Characterization of a quartz crystal microbalance with simultaneous mass and liquid loading. Analytical Chemistry, 63(20):2272–2281, 1991.

[8] Adam LJ Olsson, Henny C van der Mei, Diethelm Johannsmann, Henk J Busscher, and Prashant K Sharma. Probing colloid–substratum contact stiffness by acoustic sensing in a liquid phase. Analytical chemistry, 84(10):4504–4512, 2012.
[9] SJ Geelhood, CW Frank, and K Kanazawa. Transient quartz crystal microbalance behaviors compared. Journal of the Electrochemical Society, 149(1):H33–H38, 2002.
[10] Stanford Research Systems. QCM200 quartz crystal microbalance digital controller: operation and service manual. 2004.
[11] Yazan Hussain, Jacqueline Krim, and Christine Grant. Ots adsorption: A dynamic qcm study. Colloids and Surfaces A: Physicochemical and Engineering Aspects, 262(1):81–86, 2005.
[12] DANIEL E GOTTSCHLING, ROBERT D GROBER, and MICHAEL SAILOR. Detection of biological warfare agents. 2000.
[13] A Arnau, T Sogorb, and Y Jiménez. Circuit for continuous motional series resonant frequency and motional resistance monitoring of quartz crystal resonators by parallel capacitance compensation. Review of scientific instruments, 73(7):2724–2737, 2002.
[14] Shannon L Snellings, Jason Fuller, and David W Paul. Response of a thickness-shear-mode acoustic wave sensor to the adsorption of lipoprotein particles. Langmuir, 17(8):2521–2527, 2001.
[15] BiolinScientific / Q-Sense, Hängpilsgatan 7, SE-426 77 Västra Frölunda, Sweden, `http://www.q-sense.com/`.
[16] Xiaodi Su, Ying-Ju Wu, and Wolfgang Knoll. Comparison of surface plasmon resonance spectroscopy and quartz crystal microbalance techniques for studying dna assembly and hybridization. Biosensors and Bioelectronics, 21(5):719–726, 2005.
[17] Wendy YX Peh, Erik Reimhult, Huey Fang Teh, Jane S Thomsen, and Xiaodi Su. Understanding ligand binding effects on the conformation of estrogen receptor α-dna complexes: A combinational quartz crystal microbalance with dissipation and surface plasmon resonance study. Biophysical journal, 92(12):4415–4423, 2007.